Circulation Research

ORIGINAL RESEARCH

De Novo Germline and Somatic Variants Convergently Promote Endothelial-to-Mesenchymal Transition in Simplex Brain Arteriovenous Malformation

Hao Li,* Yoonhee Nam,* Ran Huo,* Weilun Fu,* Biaobin Jiang, Qiuxia Zhou, Dong Song, Yingxi Yang, Yuming Jiao, Jiancong Weng, Zihan Yan, Lin Di, Jie Li, Jie Wang, Hongyuan Xu, Shuo Wang, Jizong Zhao, Zilong Wen, Jiguang Wang, Yong Cao

RATIONALE: Brain arteriovenous malformations (bAVMs) are abnormal entanglement of blood vessels in brain, with direct connections from arteries to veins, lacking functional capillary bed. Although several somatic mutations were reported, the molecular mechanism and genetic disposition of bAVM remain poorly understood.

OBJECTIVE: We aim to identify transcriptional anomalies and critical functional pathways in bAVM lesions and explore their association with key de novo germline and somatic variants in bAVM patients.

METHODS AND RESULTS: We established a comprehensive bAVM dataset from 269 patients, by performing single-cell sequencing of 17 bAVM lesions, whole-exome sequencing of germline DNA from 60 case-unaffected-parental trios, and genomic/transcriptomic sequencing of 231 bAVM lesions. We found abnormal expression of endothelial and mesenchymal markers in bAVM at both bulk and single-cell level, which was validated by flow cytometric analysis and immunofluorescence staining, suggesting an involvement of endothelial-to-mesenchymal transition (EndMT) process in AVM (arteriovenous-malformation-like). Using data from the 60 trios, we identified nonsynonymous de novo germline mutations affecting 46 genes, including *EXPH5* (detected in 2 independent cases), and vessel-related genes, such as *EPAS1* and *ENG*. Interestingly, knockdown of *epas1* in zebrafish embryo showed AVM-like phenotype exclusively in brain. Subsequent computational and experimental analyses demonstrated that expression of genes affected by de novo germline mutations was enriched in vascular cell types and was involved in EndMT-relevant behaviors including cell migration, angiogenesis, and cell marker transition. Moreover, we detected somatic *KRAS* mutations in 129 of 179 (72%) cases and showed that *KRAS* mutations were associated with bleeding as the first symptom (P=0.0072). Following experimental studies demonstrated that *KRAS* mutations independently regulated EndMT features, consolidating the involvement of EndMT in this disease. Lastly, we showed that lovastatin reversed EndMT features in vitro and ex vivo.

CONCLUSIONS: Our results suggest the convergent role of de novo germline mutations and somatic mutations in regulating EndMT in bAVM and provided a potential therapeutic option.

GRAPHIC ABSTRACT: An online graphic abstract is available for this article.

Key Words: computational biology ■ germ-line mutation ■ high-throughput nucleotide sequencing ■ intracranial arteriovenous malformations

In This Issue, see p 821 | Meet the First Author, see p 822

Correspondence to: Jiguang Wang, PhD, Division of Life Science and Department of Chemical and Biological Engineering, the Hong Kong University of Science and Technology, Clear Water Bay, Hong Kong SAR, China, Email jgwang@ust.hk; or Yong Cao, MD, Neurosurgery, Beijing Tiantan Hospital, Capital Medical University, 119 S Fourth Ring Rd W, Fengtai District, Beijing, China, Email caoyong@bjtth.org
*H. Li, Y. Nam, R. Huo, and W. Fu contributed equally.
The Data Supplement is available with this article at https://www.ahajournals.org/doi/suppl/10.1161/CIRCRESAHA.121.319004.
For Sources of Funding and Disclosures, see page 838.
© 2021 American Heart Association, Inc.
Circulation Research is available at www.ahajournals.org/journal/res

Downloaded from http://ahajournals.org by on November 3, 2021

ORIGINAL RESEARCH

Novelty and Significance

What Is Known?

- Germline mutations such as *ENG*, *SMAD4*, and *ACVRL1* are associated with hereditary vascular malformation syndromes.
- Somatic mutations in *KRAS* and *BRAF* genes have been identified in endothelial cells of brain arteriovenous malformations (bAVMs) from patients with no family history.
- Activating somatic *KRAS* mutations in the endothelium leads to AVM-like (arteriovenous-malformation-like) phenotypes in mouse and zebrafish models.

What New Information Does This Article Contribute?

- Whole-exome sequencing of case-unaffected-parental bAVM trios revealed de novo germline mutations in *ENG*, *JUP*, *EXPH5*, and *EPAS1*, and subsequent in vivo study showed that *epas1*-morpholino induced brain-specific vascular malformation in zebrafish.
- Comprehensive multiomics and experimental studies demonstrated that de novo germline and somatic variants convergently promote endothelial-to-mesenchymal transition in simplex bAVM, and lovastatin treatment reverses the features of endothelial-to-mesenchymal transition in vitro and ex vivo.
- Somatic *KRAS* mutation frequently occurs in bAVMs with bleeding as the first symptom.

bAVMs contribute significantly to intracranial hemorrhage in children and young adults. Recently, somatic *KRAS* mutations were observed in bAVMs, and subsequent studies demonstrated that it can cause bAVMs in vivo through active MEK signaling. However, the clinical relevance of the mutation was unknown, and the contribution of de novo germline mutations to simplex bAVMs was largely overlooked. Here, we generated a dataset constituting of transcriptomic profiling of over 13 000 single cells from bAVM lesions, genome and transcriptome sequencing data from over 250 bAVM patients, and whole-exome sequencing data for 60 bAVM case-unaffected-parental trios. This comprehensive dataset allowed us to investigate molecular mechanism of bAVM at a single-cell level and interrogate the effects of somatic and de novo germline mutations for the first time. We identified crucial de novo germline mutations occurring in genes including *ENG*, *JUP*, *EXPH5*, and *EPAS1*, which are potentially associated with bAVM pathogenesis. Specifically, knockdown of *epas1* in zebrafish caused vascular malformations in the brain. In addition, somatic *KRAS*-mutant cases were more prone to experience bleeding as the first symptom. Lastly, lovastatin reversed endothelial-to-mesenchymal transition features in vitro and ex vivo.

Nonstandard Abbreviations and Acronyms

AVM	arteriovenous malformation
bAVM	brain arteriovenous malformation
DNM	de novo germline mutation
EC	endothelial cell
EndMT	endothelial-to-mesenchymal transition
FDR	false discovery rate
HUVEC	human umbilical vein endothelial cell
NES	normalized enrichment score
RNA-seq	RNA sequencing
SA	superficial temporal artery
SNP	single-nucleotide polymorphism
VAF	variant allele frequency
WES	whole-exome sequencing
WT	wild type

Brain arteriovenous malformations (bAVMs) are abnormal entanglement of blood vessels in brain, responsible for 3% to 4% of intracranial hemorrhage in children.[1] The disease lesion of AVM (arteriovenous-malformation-like) is called nidus, which generates direct connections from the arteries to the veins lacking a functional capillary bed. About 95% of bAVM cases have no known family history, and their pathogenesis is unclear. Recent studies found somatic *KRAS* mutations in bAVMs with frequencies ranging from 28.5% to 76.2% across different studies.[2–7] In these studies, the enrolled number of AVM cases was typically small, limiting the discovery of this mutation's clinical associations. Subsequent functional studies proposed that bAVMs develop as a consequence of somatic mutations in endothelial cells (ECs), and in vivo experiments demonstrated that endothelial-specific gain of these mutations is sufficient to induce bAVM-like phenomenon in mice and zebrafish models.[3,8] While the driving role of *KRAS* in bAVM has been well investigated, its clinical implications and molecular mechanisms are still not fully understood. Moreover, genetic factors of *KRAS*-WT (wild type) cases remain unexplored.

Anomalies of ECs, including differentiation, polarization, and mesenchymal behaviors, were observed in bAVM lesions, and manipulated genetic mutation in ECs caused bAVM-like phenotype in animal models.[8–10] However, critical genetic determination factors and key transcriptional pathways of the AVM genesis process are still unclear. Great efforts have been devoted to study

Downloaded from http://ahajournals.org by on November 3, 2021

the disease lesion of bAVMs through RNA sequencing (RNA-seq) that implied the association of KRAS/MAPK (mitogen-activated protein kinase) signaling, inflammation, and impaired vascular wall integrity with bAVM lesions.[11,12] Nonetheless, these approaches were limited to characterizing one cell type[11] or averaged gene expressions of the whole tissue composed of various types of cells,[12] lacking the resolution to decouple the complexity of this disease. In contrast, single-cell technology that allows detailed analysis of the heterogeneity and molecular changes of individual cells may lead to a better understanding of the disease mechanism.[13,14]

In this study, we aim to establish a comprehensive dataset of bAVM using multiomics sequencing. On one hand, enlightened by the study of de novo germline mutations (DNMs) in other simplex human genetic disorders[15,16] and considering that bAVM patients are typically young, we hypothesized that DNMs might also contribute to the pathogenesis of simplex bAVMs. Thus, we identify the anomalies of bAVM ECs and investigate the underlying genetic causes from both somatic and germline alterations. On the other hand, we perform both bulk and single-cell sequencing to characterize the transcriptional program of AVM ECs, based on which we report the key process driving AVM genesis.

METHODS

Data Availability

The raw data of this study are available from the Genome Sequence Archive with accession number HRA001250 upon reasonable request. For the software and research materials, please see the Major Resources Table in the Data Supplement. Details of Materials and Methods are described in the Data Supplement.

RESULTS

Patients

A total of 269 simplex bAVM patients from January 2016 to May 2020 were included in this study (Table I in the Data Supplement). Of those, 239 had fresh-frozen or fresh-resected nidus tissue and 154 had matched blood. We performed bulk RNA-seq on the bAVM nidus of 66 patients and single-cell RNA-seq on 17 patients to profile transcriptomic pattern of cells in bAVM lesions. Whole-exome sequencing (WES) was performed on germline DNA of 60 patients together with the matched unaffected parental blood for the identification of DNMs. In addition, 219 nidus tissues were used for WES, amplicon sequencing, and droplet digital polymerase chain reaction to identify somatic mutations (Figure 1A through 1C). Flow cytometry, immunofluorescence staining, electron microscopy, and patient-derived EC culture were also carried out to characterize the nidus. For control purpose, non-nidus vessels were obtained from 8 bAVMs during standard procedure of craniotomies and bAVM resection. These vessels included superficial temporal arteries (SAs), scalp SAs, feeding arteries, and draining veins.

As patient-level control, we analyzed brain vessels from 11 patients undergoing temporal lobe resection for non-AVM epilepsy and SAs from 4 non-AVM nonepilepsy patients during standard neurosurgical procedures like pterional craniotomy for aneurysm clipping. Sample details are provided in Table I in the Data Supplement.

Endothelial-to-Mesenchymal Transition in BAVMs

We performed bulk RNA-seq on nidus from 66 bAVM cases and control vessels from 7 non-bAVM epilepsy patients. Gene set enrichment analysis found significantly lower expression of brain endothelial markers[17] in bAVMs than control (Figure 2A). Notably, *ICAM2*, *FLT1*, and *KDR* were among the most downexpressed genes (Figure 2B). To explore bAVM ECs at a single-cell level, we performed single-cell RNA-seq on nidus from 17 patients. A total of 13 328 high-quality single cells were clustered and visualized (Figure 2C; Figure IA and IB in the Data Supplement). We detected 3 distinct EC clusters and 1 mural/fibroblast cluster. Unexpected expression of mesenchymal markers was observed in EC1-EC3, in contrast to ECs from non-AVM human brain[18] (Figure 2D; Figure IC and ID in the Data Supplement). Other than the ECs, we also investigated the abnormal subclusters in mural and fibroblast cells. Particularly, we merged AVM EC and mural/fibroblast clusters (EC1-EC3 and mural/fibroblast in Figure 2) with EC (control-EC) and pericyte cells (control-pericytes) from the control[18] into one uniform manifold approximation and projection (Figure IIA in the Data Supplement). Control-EC cluster majorly overlapped with AVM-EC1, with a little overlap with the AVM-EC2 cluster. Control-pericyte cluster overlapped with mural/fibroblast cluster from AVM lesions. However, within the mural/fibroblast cluster, we identified a subcluster of cells that did not overlap with control-pericyte (Figure IIB in the Data Supplement). We termed this subcluster AVM-specific mesenchymal cells. Interestingly, the AVM-specific mesenchymal cell cluster simultaneously expressed *CLDN5* (EC marker), *MYL9* (smooth muscle cell marker), *PDGFRB*, and *RGS5* (pericyte markers), implying that the cluster may represent a novel group of cells carrying expression features of both endothelial and mesenchymal cells (Figure IIC in the Data Supplement). Further pathway enrichment analysis showed that expression level of the genes associated with blood vessel diameter maintenance, regulation of tube diameter, and muscle contraction pathways were significantly higher in the AVM-specific mesenchymal cell cluster (Figure IID and IIE in the Data Supplement). This interesting cluster provides new evidence of endothelial-to-mesenchymal transition (EndMT) in bAVM. Collectively,

Downloaded from http://ahajournals.org by on November 3, 2021

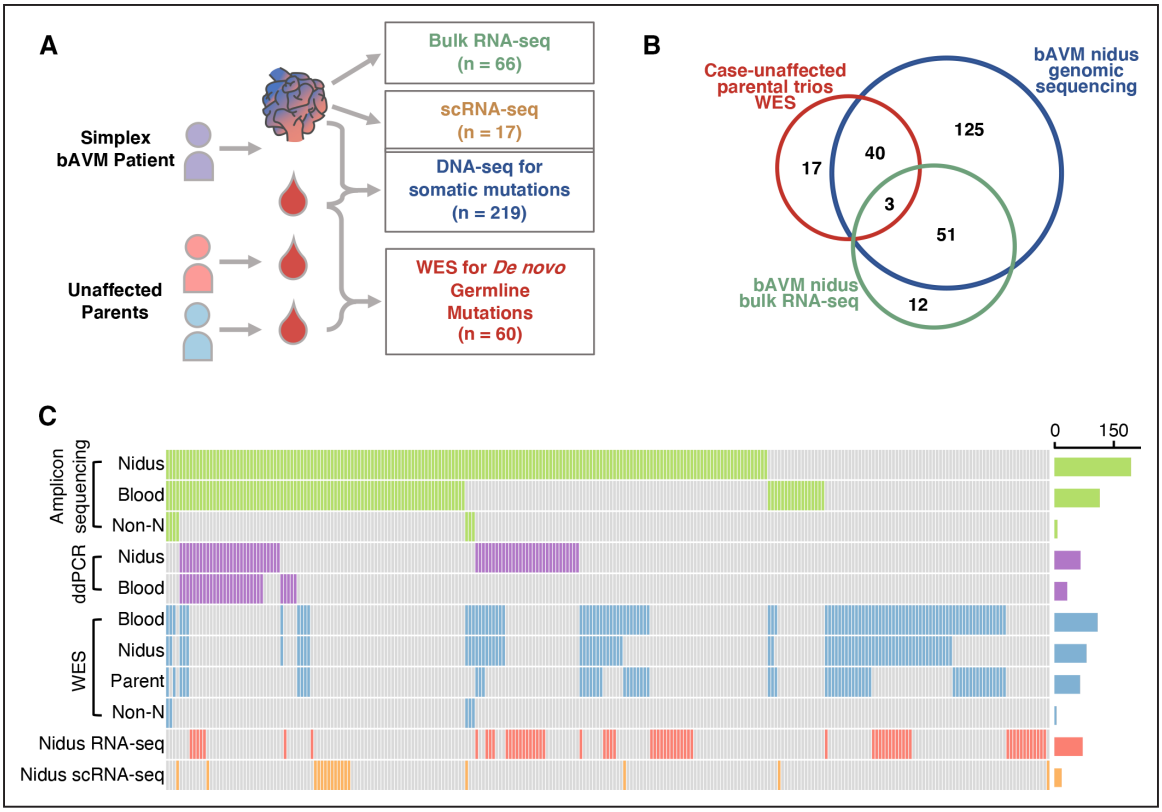


Figure 1. Multiomics profiling characterized somatic and de novo germline alterations of brain arteriovenous malformations (bAVMs).

A, Multiomics data collection of simplex bAVM patients and matched unaffected parents. Different sequencing technologies performed on the specimens are shown in the boxes with the total number of patients annotated in parenthesis. DNA sequencing (DNA-seq) for somatic mutations includes whole-exome sequencing (WES), amplicon sequencing (amplicon-seq), and droplet digital polymerase chain reaction (ddPCR). **B**, Statistics of the bulk sequencing samples. **C**, Summary of samples by sample type and sequencing protocol. Each column represents a patient. Non-N, non-nidus vessel samples; Parent, parent blood DNA; RNA-seq, RNA sequencing; and scRNA-seq, single-cell RNA sequencing.

we reasoned that bAVM might undergo the process of EndMT.[19,20]

To verify the EndMT hypothesis, we utilized fluorescence-activated cell sorting to purify cells using CD31 (cluster of differentiation 31; an endothelial marker) and α-SMA (alpha-smooth muscle actin; a commonly used mesenchymal marker), in independent bAVM cases compared with non-AVM epilepsy control. Interestingly, we found that α-SMA+ CD31+ CD45− cells constituted on average 24.8% (SEM, ±6.1; n=9) among all CD31+ CD45− (endothelial) cells in bAVM nidus, significantly higher than the control (mean±SEM, 3.8±1.3; n=4; Figure 2E; Figure III in the Data Supplement; Mann-Whitney nonparametric test, *P*=0.0028). Considering that the artery/vein ratio might be a cofounding factor introducing bias to the current results, we next performed multicolor immunofluorescent staining to examine marker genes at protein level including α-SMA, SLUG, (SNAI2, snail family transcriptional repressor 2), TAGLN (Transgelin), S100A4, and MYL9 in bAVM endothelium in comparison to SAs. The mesenchymal markers were remarkably stained in the endothelium lining the lumen of bAVM lesions but were seldomly expressed in control endothelium, further demonstrating the occurrence of EndMT in lesions of human bAVM (Figure 2F).

Detection of DNMs

Since germline variants in Hereditary Hemorrhagic Telangiectasia (*HHT*) genes could induce hereditary syndromes that were hallmarked by bAVM,[21,22] we hypothesized that simplex bAVM patients without family history might develop as the consequence of DNMs that occurred in germ cells or during early embryonic development. To test this hypothesis, deep WES was performed for 60 case-unaffected-parental trios to detect DNMs in bAVM patients. The sequencing depth of these samples was summarized in Figure IVA in the Data Supplement. Due to intrinsic sampling bias (ie, parental DNAs of younger cases were easier to be acquired), the average AVM diagnosis age of patients enrolled for DNM study was younger than the rest of the enrolled cases in this study (Figure IVB in the Data Supplement). Furthermore, the DenovoSAVI pipeline was developed and used for DNM identification. As a result, a total of 63 DNMs were detected (with 49 confirmed by mass spectrometry or Sanger sequencing), averaging to 1.05 DNMs (63/60) per exome per generation (Figure 3A; Figure IVC and IVD in the Data Supplement; Table II in the Data Supplement). This number is compatible with the mutation rate

Downloaded from http://ahajournals.org by on November 3, 2021

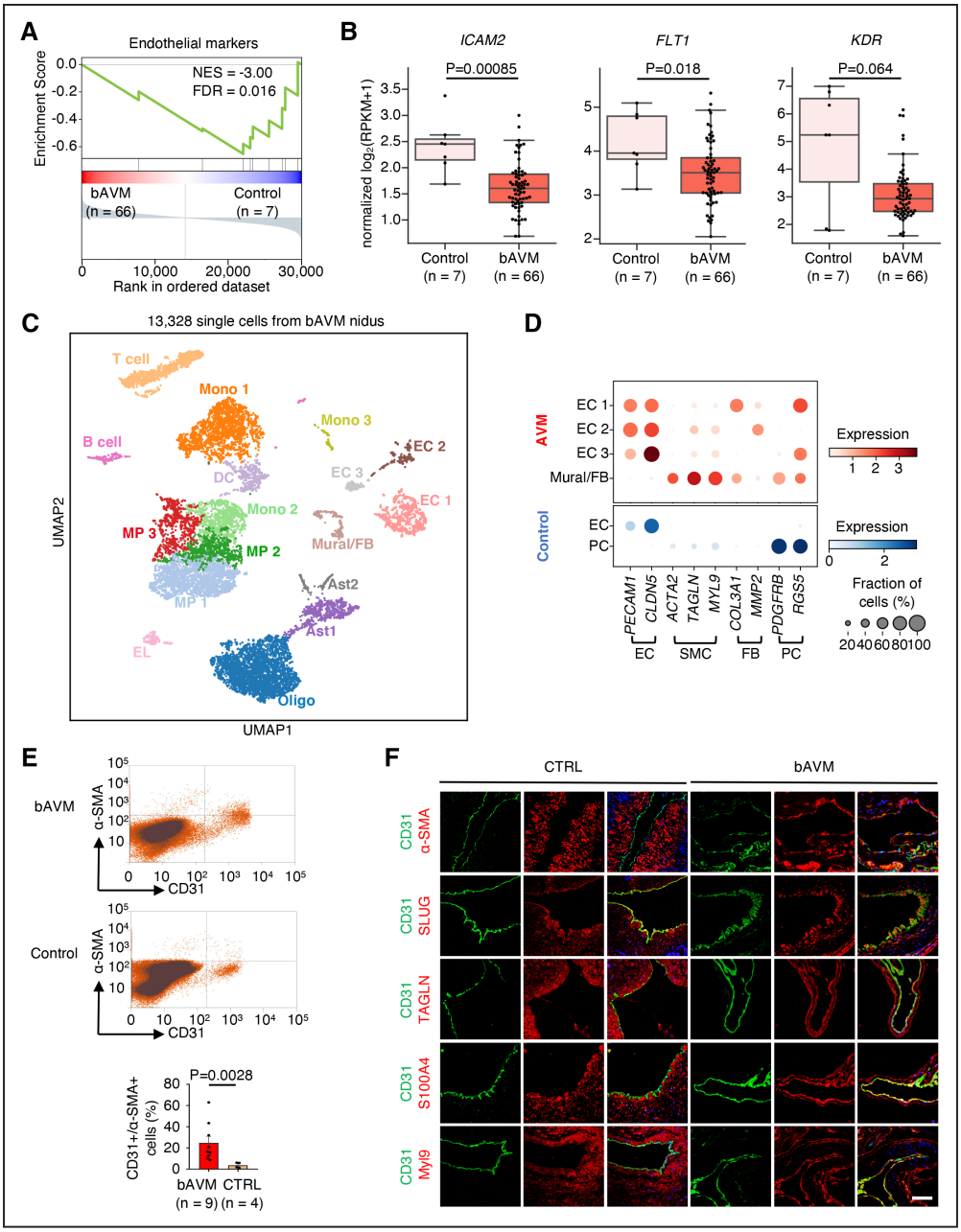


Figure 2. Bulk and single-cell sequencing revealed endothelial-to-mesenchymal transition in brain arteriovenous malformation (bAVM) lesions.

A, GSEA for brain endothelial marker genes (n=9) in 66 bAVM bulk samples compared to 7 control vessels from epilepsy patients. **B**, Normalized $\log_2$ expression of 3 brain endothelial marker genes that had lower expression level in bAVMs. The central line of each box represents the median value. Lower and upper boundaries represent the 25th and 75th percentiles. The ends of whisker bars represent 1.5× the interquartile range. *P* by Wilcoxon rank-sum test. **C**, Uniform manifold approximation and projection (UMAP) of 13328 cells from 17 bAVM patients colored by cell types. **D**, Expression level of endothelial cells (ECs) and mural and fibroblast cell clusters in AVM cohort (red) and Allen database (blue). Endothelial cell (EC), smooth muscle cell (SMC), fibroblast (FB), and pericyte (PC) marker genes are shown. Color intensity indicates mean log normalized expression in each cluster. Dot size indicates fraction of cells expressing the gene in each cluster. **E**, Flow cytometric analysis of expression of α-SMA in CD31+ cells isolated from bAVM (n=9) and control blood vessels of epilepsy brain tissues (n=4). The upper subpanel is the representative flow cytometric chart of bAVM and control blood vessel. The T bars represent SEM *P* by Mann-Whitney nonparametric test. **F**, Expression of CD31 (green, EC marker) and mesenchymal markers (red) in bAVM nidus and control SAs by immunofluorescence staining. Scale bar, 50 μm. Ast indicates astrocytes; α-SMA, alpha-smooth muscle actin; AVM, arteriovenous malformation; CD31, cluster of differentiation 31; Ctrl, control; DC, dendritic cells; EL, erythroid-like cells; FDR, false discovery rate; Mono, monocytes; MP, macrophages; NES, normalized enrichment score; Oligo, oligodendrocytes; RPKM, reads per kilobase of transcript per million mapped reads; SLUG, SNAI2 snail family transcriptional repressor 2; and TAGLN, transgelin.

estimated by other methods (ranging from 1.1×10^{-8} to 2.5×10^{-8} per site per generation),[23–25] suggesting that AVM might not be driven by higher germline mutation rate. However, the missense-to-synonymous ratio was 3.75 (45/12), indicating a positive selection compared with neutral expectation (2.23 missense mutations

Downloaded from http://ahajournals.org by on November 3, 2021

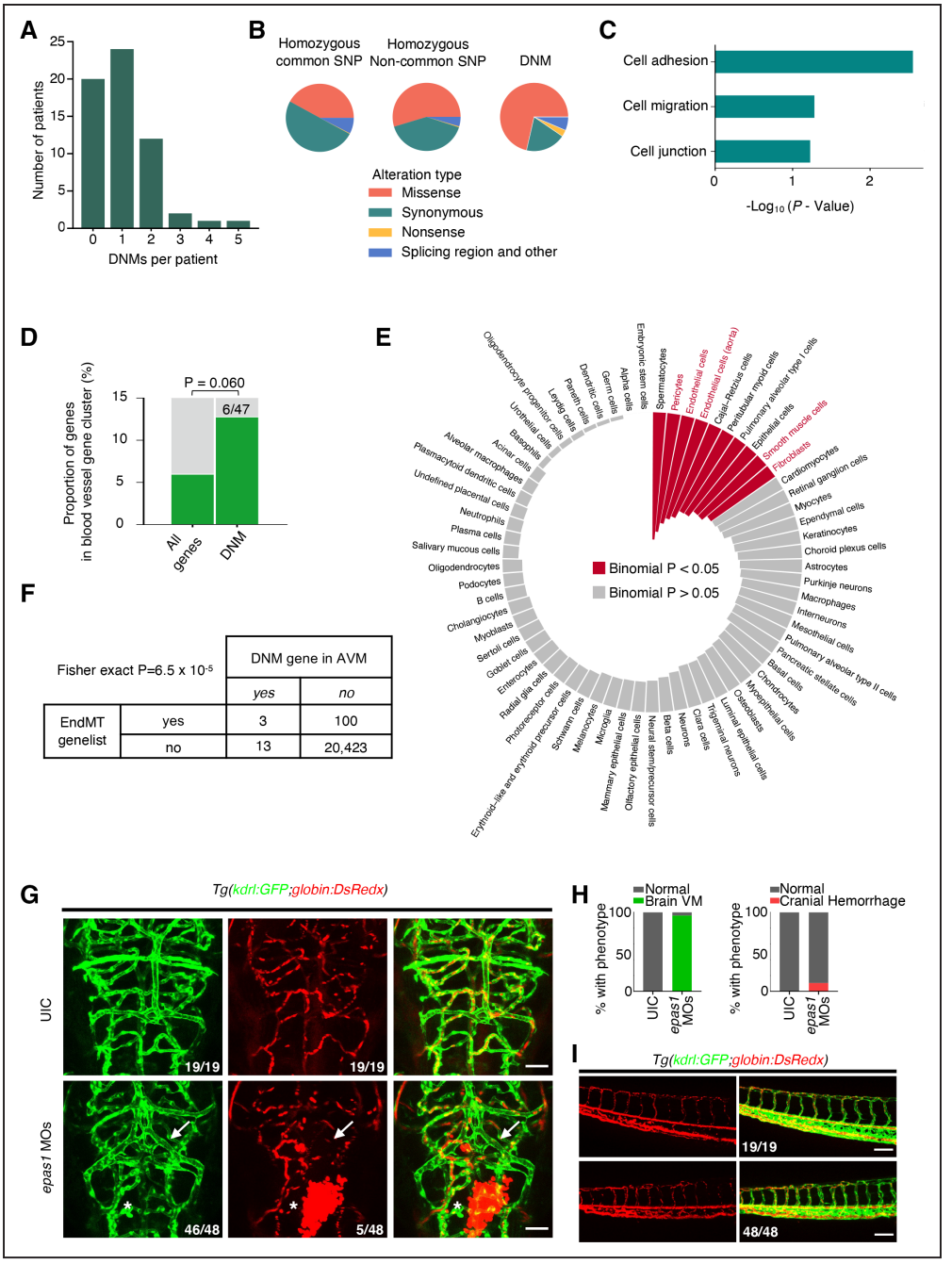


Figure 3. Genomic sequencing study of case-unaffected parental trios uncovered the landscape of de novo germline mutations (DNMs) in brain arteriovenous malformations.

A, Distribution of DNMs per patient in the 60 case-unaffected parent trios. **B**, Distribution of alterations in NH–single-nucleotide polymorphism (SNP) and DNMs. **C**, Gene ontology pathway analysis on 46 DNM genes. *P* by modified Fisher exact P (EASE score) from DAVID. **D**, Enrichment of 46 DNM genes in blood vessel from GTEx database compared with random (all genes). *P* by binomial exact test (hypothesized probability of success, 1116/18659). **E**, Expression enrichment of 46 DNM genes in each cell type from the Panglao database. Length of bar represents enrichment *P* and those <0.05 are colored in red. Cell types associated with blood vessel are colored in red. *P* by binomial exact test. **F**, Fisher exact test contingency table for association of 16 DNMs (Table) and endothelial-to-mesenchymal transition (EndMT). Total number of coding genes used for DNM detection is shown. **G**, Representative confocal images for the brain of *epas1* morpholinos (MOs) injected *Tg(kdrl:GFP;globin:DsRedx)* embryos and uninjected control (UIC). Arrows indicate kdrl:GFP+ vessel ECs with altered morphology, while the cranial hemorrhage indicated by accumulated globin:DsRedx+ red blood cells is pointed out by the asterisk; dorsal views. Scale bars, 50 μm. **H**, Quantification of percentage of embryos with indicated phenotype in each condition. **I**, Representative confocal images for the trunk of *epas1* MOs injected embryos and UIC; lateral views. Scale bars, 100 μm. All images taken at 60 to 70 hpf. Data are representative of 3 independent experiments. n/n=number of embryos with representative phenotype/total number of embryos examined. AVM indicates arteriovenous malformation; GFP, green fluorescent protein; GTEx, the genotype-tissue expression; and VM, vascular malformation.

Downloaded from http://ahajournals.org by on November 3, 2021

expected to occur per synonymous mutation).[26] In addition, we calculated the ratio of different variants in new homozygous single-nucleotide polymorphism (SNP; ie, heterozygous in parents but homozygous in proband) and found that both missense and nonsense variants were remarkably enriched in DNMs compared with that in new homozygous SNP for both common and non-common SNPs. These results collectively implied the potential involvement of DNM in AVM's disease genesis (Figure 3B).

Characterization and Prioritization of DNMS

In the following analyses, synonymous mutations and common SNPs (allele frequency ≥1% in 1000Genomes population) were excluded, leaving 48 DNMs affecting 46 genes (Table III in the Data Supplement). Notably, *EXPH5* gene was altered in 2 independent patients, and other genes were unique to each proband. Four mutations were nonsense or splicing site mutations with higher functional impact, including *EXPH5* (R1111*), *JUP* (Q9*), *CHEK2* (c.1008+2T>G), and *ENG* (c.360+1G>A). *JUP* encodes plakoglobin—a protein closely related to β-catenin that links desmosomal cadherins to intermediate filaments and can also substitute for β-catenin in adherens junctions.[27] *ENG*—a coreceptor for TGF-β (transforming growth factor beta) in EC—is reported contributing to the pathology of HHT1 (hereditary hemorrhagic telangiectasia type 1), which is featured by bAVMs.[28] Hence, the patient with *ENG* (c.360+1G>A) variant is likely a de novo HHT case without family history. This *ENG* splice site mutation was reported causing a reduction in the level of functional endoglin.[29] *EXPH5* encodes a ras-related protein Rab-27B effector protein Slac2-b. Mutations in this gene have been associated with epidermolysis bullosa, an inherited skin fragility disorder, and Slac2-b knockdown reduced keratinocytes adhesion.[30] Among the 48 DNMs, 23 variants were found with dbSNP reference SNP (rs) numbers, but based on population allele frequencies from public database,[31,32] all of them were rare SNPs (allele frequencies below 0.1% in population). According to the genotyping validation (mass spectrometry or Sanger sequencing) performed on these 23 SNP-numbered DNMs, 18 of 20 successfully genotyped variants were confirmed to be de novo (Table III in the Data Supplement).

We then performed gene ontology enrichment analysis and found these 46 genes were enriched in cell adhesion, cell migration, and cell junction, all of which relate to EndMT AVM phenotype (Figure 3C). To investigate tissue expression of these DNM genes, we analyzed gene expression profiles of 11 688 samples from a wide range of tissue types and defined tissue-specific gene clusters for 33 tissue types (Figure V in the Data Supplement). Interestingly, 6 genes including *EPAS1* (related to vascular remodeling[33]), *DACT1*, *EMILIN1* (functions in vascular cell maintenance and inhibits TGF-β signaling[34,35]), *ENG*, *GAS6*, and *COL1A1* were in the vessel-specific gene expression cluster, relatively higher than random (Figure 3D; binomial test P=0.060). Next, we performed cell type enrichment analysis (Figure VIA in the Data Supplement)[36] and found most significant involvement of cell types constituting blood vessel and surrounding tissues, including ECs, pericytes, smooth muscle cells, and fibroblasts using both adult and nonadult single-cell datasets (Figure 3E; Figure VIB and VIC in the Data Supplement). These evidences collectively demonstrated that the gene list we identified from the 60 trios contained an elevated number of bAVM-associated genes.

In addition, we used in silico mutagenesis and protein homology modeling to construct a series of 3-dimensional structural models of the proteins in WT and mutant type. Limited by the availability of the protein structure database and accuracy of homology remodeling, this analysis was performed in 7 variants. We observed that most of the analyzed DNMs occurred on functional sites of proteins, and these mutations often changed local charge distributions that might affect protein-protein interactions, protein-ligand interactions, protein-RNA interactions, and protein-DNA interactions (Figure VII in the Data Supplement; Table III in the Data Supplement).

To identify bAVM-relevant DNM genes, we considered both mutational impact and the above enrichment analyses and eventually prioritized 16 genes in the Table as candidate bAVM-associated genes. Interestingly, we found that patients carrying DNMs in these genes had a higher chance to have epilepsy as the first symptom (Fisher exact test, P=0.023; Figure VIII in the Data Supplement). Remarkably, 3 (ie, *JUP*, *ENG*, and *COL1A1*) of the 16 genes were included in the known EndMT gene list,[37] implying that DNMs might regulate the process of EndMT in bAVMs (Fisher exact test, $P=6.5\times10^{-5}$; Figure 3F).

Knockdown of EPAS1 in Zebrafish Alters Brain Vascular Morphology and Causes Cranial Hemorrhage

We then performed in vivo experiments on zebrafish (*Danio Rerio*) by injecting morpholino against the selected candidate gene into *Tg(kdrl:GFP;globin:DsRedx)* zebrafish embryos and then evaluated the corresponding phenotype in morphants at 60 to 70 hours post-fertilization by visualizing the green fluorescent protein (GFP)-positive ECs and DsRedx-positive red blood cells.

In particular, we set out to study a DNM gene that was vessel specific in our tissue-level expression analysis and reported to be related to vascular remodeling in mouse, *EPAS1*. *EPAS1* has 2 orthologs in zebrafish, *epas1a* and *epas1b*. Previous studies have shown unaffected trunk vessel formation in zebrafish *epas1* mutants.[38] We reinvestigated the vasculature by coinjecting *epas1a* and *epas1b* morpholinos into the embryos of *Tg(kdrl:GFP;globin:DsRedx).* Strikingly, while *epas1* morphants indeed displayed normal trunk vasculature, their

Downloaded from http://ahajournals.org by on November 3, 2021

Table. De Novo Germline Mutations in the Prioritized 16 Genes

Patient ID	Mutation(hg19)	Codon change	Amino acid change	Gene name
A060	14:59113527A>G	gAg/gGg	E729G	*DACT1*
A060	9:139757412T>G	Agc/Cgc	S111R	*EDF1*
A061	1:39549928C>T	tCa/tTa	S13L	*MACF1*
A063	2:27305521G>A	cGa/cAa	R361Q	*EMILIN1*
A070	22:29095824A>T	…	Splice-donor	*CHEK2*
A071	2:46609156C>T	Cgg/Tgg	R739W	*EPAS1*
A074	9:130591965C>T	…	Splice-donor	*ENG*
A076	11:620367C>T	cGt/cAt	R270H	*CDHR5*
A077	17:39928082G>A	Cag/Tag	Q9*	*JUP*
A079	11:108380449G>C	Cct/Gct	P1929A	*EXPH5*
A081	17:48269343T>C	Aga/Gga	R676G	*COL1A1*
A082	11:404125A>C	Aag/Cag	K754Q	*PKP3*
A083	13:114538531A>T	Tgt/Agt	C223S	*GAS6*
A083	3:147128347G>A	Gct/Act	A150T	*ZIC1*
A087	11:108382903T>A	Aga/Tga	R1111*	*EXPH5*
A093	10:24908804C>T	Gat/Aat	D674N	*ARHGAP21*
A095	1:35370303G>C	Cac/Gac	H228D	*DLGAP3*
A095	1:35370304G>T	caC/caA	H227Q	*DLGAP3*

The variants in patient A095 were in phase; that is, both were observed in the same reads.

brains showed robust and significant vascular malformations (Figure 3G through 3I), in which reticulated vasculature was formed (46/48) and some were accompanied with severe bleeding (5/48). These observations indicate that knockdown of the *EPAS1* gene may directly act to drive bAVM-like brain vascular malformations in vivo.

Association Between DNMs and ENDMT

To explore the association between DNMs and EndMT, we manipulated human umbilical vein endothelial cells (HUVECs) to study the function of *JUP*, *ENG*, and *EXPH5*, selected endothelial genes with high-impact DNMs (Figure IX in the Data Supplement; Table IV in the Data Supplement). Gene set enrichment analysis of RNA-seq in *JUP* and *ENG* knockdown HUVECs confirmed the occurrence of EndMT using not only the known upexpressed-in-EndMT gene set (*JUP*: normalized enrichment score [NES], 3.004; false discovery rate [FDR], 0.010; *ENG*: NES, 3.133; FDR, <0.001) but also the known downexpressed-in-EndMT gene set (*JUP*: NES, −4.303; FDR, <0.001; *ENG*: NES, −4.552; FDR, <0.001; Figure 4A; Figures X and XI in the Data Supplement). For *EXPH5* knockdown HUVECs, we found an increase in upexpressed-in-EndMT genes (NES, 2.798; FDR, 0.068) but not the decrease in downexpressed-in-EndMT genes, probably indicating a partial EndMT in EXPH5 knockdown HUVECs[39] (Figure XIE through XIG in the Data Supplement).

We further performed immunofluorescent staining and observed increased expression of mesenchymal markers (α-SMA and TAGLN [transgelin]) and decreased expression of CD31 in HUVECs with *JUP* and *ENG* knockdown (Figure 4B; Figure XII in the Data Supplement). In consistency with RNA-seq, we found *EXPH5* knockdown HUVECs showed increased level of α-SMA and TAGLN but no significant change in CD31. We also observed enhanced cell migration in HUVECs with *JUP*, *ENG*, and *EXPH5* knockdown by wound healing analysis (Figure 4C). Moreover, fibrin gel bead assay showed that knockdown of DNM genes inhibited vascular-like structure formation in HUVECs (Figure 4D). Altogether, these evidences confirmed the involvement of DNM genes in regulating EndMT in vitro.

KRAS Mutation and ENDMT

Recent studies identified somatic *KRAS* and *BRAF* mutations in bAVM[2–7] and observed activation of MAPK-ERK (extracellular signal regulated kinase) signaling pathway, as well as expression changes of EndMT-related genes in $KRAS^{G12V}$-expressing HUVECs.[2] To explore the underlying association among somatic alterations, DNMs and EndMT, we examined bAVM nidus from 219 patients for detecting somatic mutations. We first used WES from 75 nidus with matched blood to identify somatic variant candidates. We found *KRAS* G12D, G12V, G12A, and Q61H mutations with variant allele frequency (VAF) ranging from 1.87% to 10.26% (Figure XIII in the Data Supplement). Although median coverage of AVM WES was >250×, coverage for *KRAS* and *BRAF* hot spots was below 120×, which may have limited the detection of low-frequency mutations (Figure XIV in the Data Supplement). We, therefore, performed amplicon sequencing (median coverage, 13000×) targeting *KRAS* c.35G and c.34G in 179 bAVM nidus and 106 blood. A model using β-binomial distribution was developed to identify variants with low allelic frequency (Figure XV in the Data Supplement). Using this method,

Downloaded from http://ahajournals.org by on November 3, 2021

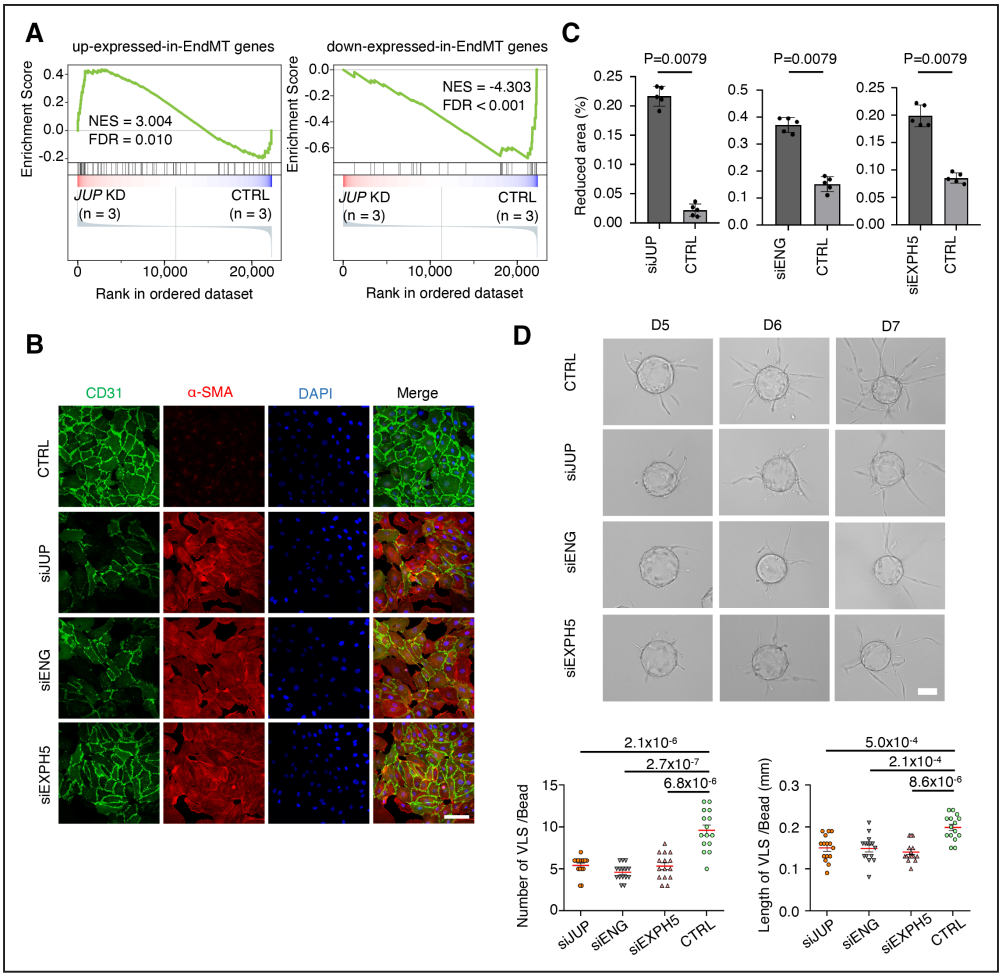


Figure 4. In vitro studies demonstrated the role of de novo germline mutations (DNMs) in promoting endothelial-to-mesenchymal transition (EndMT) in human umbilical vein endothelial cells (HUVECs).
A, GSEA of JUP-KD (knockdown) HUVECs (n=3) in EndMT gene list compared with control (n=3). **B**, Expression of mesenchymal marker (α-SMA [alpha-smooth muscle actin]) in HUVECs induced by *JUP*, *ENG*, and *EXPH5* knockdown, while CD31 was suppressed by *JUP* and *ENG* but not *EXPH5* knockdown. Scale bar, 100 μm. **C**, Reduced area of HUVECs with JUP, ENG, and EXPH5 knockdown with siRNA in comparison with that of control in wound healing analysis. The T bars represent SD (n=5). *P* by Mann-Whitney nonparametric test. **D**, Representative phase-contrast images on beads of HUVECs with *JUP*, *ENG*, and *EXPH5* knockdown in a 3-dimensional fibrin gel angiogenesis assay at days 5, 6, and 7. The number of vascular-like structure (VLS) around the beads was counted manually, and the lengths of VLSs were quantified. Data (mean±SEM) were obtained from 15 randomly selected beads in each group from 3 individual experiments. Scale bar, 100 μm. *P* by Mann-Whitney nonparametric test. α-SMA indicates alpha-smooth muscle actin; CD31, cluster of differentiation 31; CTRL, HUVECs transfected with control siRNA; DAPI, 4',6-diamidino-2-phenylindole; FDR, false discovery rate; HUVEC, human umbilical vein endothelial cells; and NES, normalized enrichment score.

KRAS mutations were identified in 69.8% (125/179) of the nidus samples with the lowest VAF 10^{-4}. Yet, 2.8% (3/106) of the blood samples were *KRAS* mutant, implying potential false discovery rate (Figure 5A; Table V in the Data Supplement).

To confirm the results via another approach, we performed droplet digital polymerase chain reaction on 61 bAVMs and 30 blood samples on 10 selected variant candidates (Figure XIIIB in the Data Supplement). While no variants were detected in blood, 41 of 42 *KRAS* variants (97.6%) detected by amplicon sequencing were confirmed by droplet digital polymerase chain reaction with high VAF correlation (Figure XVI in the Data Supplement; Pearson r, 0.952). Moreover, 2 additional *KRAS* variants (G12V and G12S) were separately detected in patients A060 and A226. In addition, 1 *BRAF* V600E (patient A228) and 1 *KRAS* Q61H variant (patient A123) were detected. Collectively, 72% (129/179) of the patients were *KRAS* mutant via WES, amplicon sequencing, or droplet digital polymerase chain reaction. This result was comparable to the previously reported incidence in the Canadian cohort.[2]

To explore the prevalence of *KRAS* mutations in non-nidus regions, SA (n=4), scalp SAs (n=3), feeding arteries (n=7), and draining veins (n=5) from 7 patients were sequenced. One patient (A084) was $KRAS^{G12D}$ mutant in nidus (VAF, 6.6%), feeding arteries (VAF, 0.24%), and draining veins (VAF, 0.69%) but *KRAS*-WT in SA (Figure 5B). All other non-nidus samples were *KRAS*-WT (Figure XVIIA and XVIIB in the Data Supplement). Our data suggested that *KRAS* mutations are enriched in the nidus and less present in nearby vessels but are unlikely occurring at distant vessels. Moreover,

Downloaded from http://ahajournals.org by on November 3, 2021

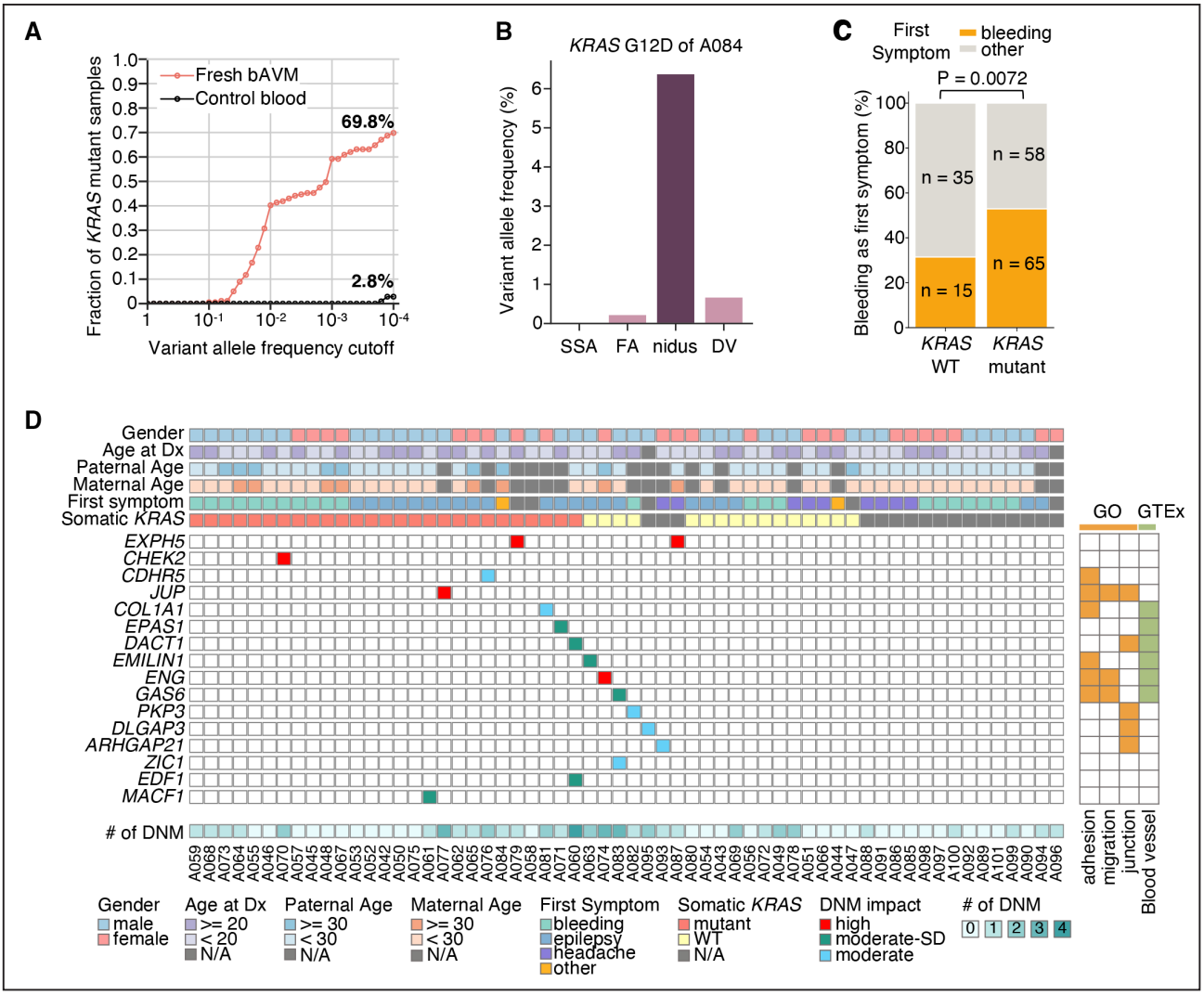


Figure 5. De novo and somatic mutational landscape of brain arteriovenous malformation (bAVM).
A, Fraction of *KRAS*-mutant samples detected by amplicon sequencing (amplicon-seq). A *KRAS*-mutant sample is identified under the criteria of Benjamini-Hochberg–adjusted $P<0.2$. The P is calculated from a 1-tailed test: whether an averaged sequencing noise is less than or equal to the VAF estimated through a posterior β-distribution (see Methods). Lines display fraction of *KRAS*-mutant samples given different lower bounds of VAF. The percentage on the right denotes the fraction of *KRAS*-mutant samples at the minimum lower bound, equivalently as the limit of detection. **B**, Amplicon-seq in patient A084 with nidus and non-nidus vessels. **C**, Ratio of patients having bleeding as the first symptom in *KRAS*-mutant and WT (wild type) groups. *KRAS* mutation determined by amplicon-seq, whole-exome sequencing (WES), or droplet digital polymerase chain reaction (ddPCR) of bAVM. P by Fisher exact test. **D**, Landscape of 60 case-unaffected parent trios. **Top**, Clinical features and somatic *KRAS* mutation. *KRAS* mutation is determined by WES, amplicon-seq, or ddPCR of bulk bAVM. **Middle**, Selected de novo germline mutation (DNM) genes. Color indicates the protein impact of the mutation. **Bottom**, Number of noncommon and nonsynonymous DNMs in each patient. **Right**, DNM genes enriched in gene ontology (GO) pathways and enriched in blood vessel from tissue-specific analysis (GTEx). High (impact), nonsense, or splicing site mutations; moderate-SD, missense mutation and predicted to be deleterious by SIFT; moderate, missense mutation. DV indicates draining vein; Dx, diagnosis; FA, feeding artery; GTEx, the genotype-tissue expression; N/A, not available; and SSA, scalp superficial temporal artery.

the large sample set in our study allowed us to explore clinical and phenotypic relevance of the somatic *KRAS* mutations. Interestingly, we found that *KRAS*-mutant cases had higher incidence of having bleeding as the first symptom (Fisher exact test, $P=0.0072$; Figure 5C). No association was observed between somatic *KRAS* mutation and preoperative radiotherapy (Fisher exact test, $P=0.3$; Figure XVIIC in the Data Supplement). Furthermore, recent study reported that 2 patients with somatic *BRAF* mutation demonstrated relatively older ages.[7] Similarly, our A228 patient with somatic *BRAF* V600E mutation (VAF, 1.03%) was diagnosed at age 43, higher than the median age 23 of all the bAVM participants in our study.

To explore the association between somatic *KRAS* mutation and DNMs, we investigated 43 cases that were enrolled in both DNM and somatic mutation study. Figure 5D showed the landscape of the 60 trios, with information on somatic *KRAS* mutations and the selected 16 DNMs. Eight of 27 *KRAS*-mutant patients also carried DNMs in the prioritized 16 genes, while 4 of 16 patients were *KRAS*-WT and de novo mutated. No

Downloaded from http://ahajournals.org by on November 3, 2021

significant trend was observed between somatic *KRAS* mutation and the DNMs.

We generated HUVECs overexpressing KRAS4B^{G12D} to explore potential role of *KRAS* in regulating EndMT. As expected, elevated phosphorylated ERK was detected in manipulated HUVECs (Figure XVIIIA in the Data Supplement). We also observed increased level of mesenchymal markers and suppression of endothelial markers in *KRAS-4B*^{G12D}-overexpressing HUVECs by Western blot (Figure 6A), immunofluorescence staining (Figure 6B; Figure XVIIIB in the Data Supplement), and qPCR (quantitative reverse transcription) (Figure XVIIIC in the Data Supplement; Table VI in the Data Supplement).

Morphologically, the cobblestone appearance of ECs was transformed into an elongated and spindle-like shape in immunofluorescence staining by KRAS activation, consistent with reported EndMT observations[40] (Figure 6B). Moreover, KRAS4B^{G12D}-HUVECs acquired an enhanced migratory ability (Figure 6C). We then blocked the MAPK-ERK pathway utilizing the MAPK-specific inhibitor U0126 and observed that KRAS4B^{G12D}-driven changes were rescued, confirming the role of MAPK-ERK signaling in mediating EndMT in HUVECs (Figure 6A through 6C). Furthermore, we analyzed KRAS^{G12D}-induced morphogenesis in a bead-based morphogenesis assay.[41] Control ECs sprouted numerous tubular vascular-like structures mimicking angiogenesis, while KRAS4B^{G12D} HUVECs exhibited sheet-like structures, rather than normal vascular elongation and lumenogenesis (Figure 6D). These results collectively confirmed the role of activating *KRAS* mutation in driving EndMT in vitro.

Lovastatin Attenuates EndMT In Vitro and Ex Vivo

Lovastatin—an agent widely used in treating lipid disorders—may inhibit EndMT in glomerular ECs.[42] To explore

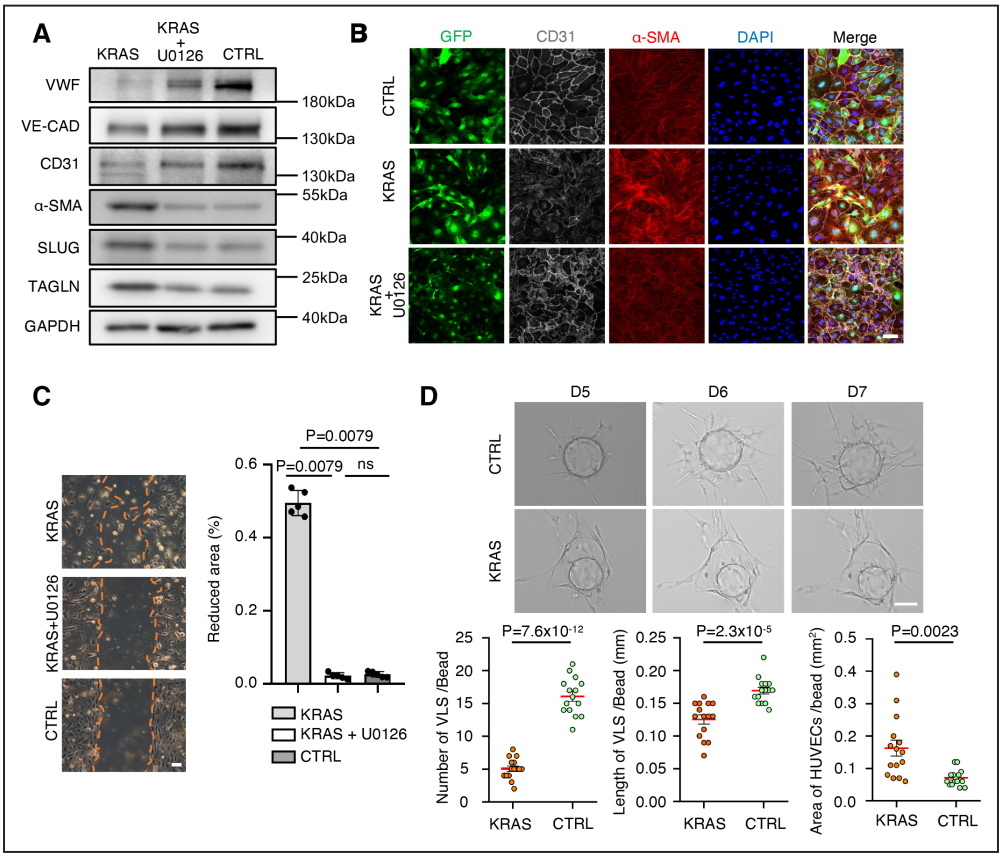


Figure 6. In vitro studies demonstrated the role of somatic *KRAS* mutations in promoting endothelial-to-mesenchymal transition in human umbilical vein endothelial cells (HUVECs).

A, Western blot of mesenchymal markers α-SMA, SLUG, and TAGLN and endothelial markers VWF, VE-CAD, and CD31 in HUVECs overexpressing KRAS4B^{G12D}, HUVECs overexpressing KRAS4B^{G12D} treated with U0126, and control. **B**, Immunofluorescence staining of CD31 and α-SMA in HUVECs. Scale bar, 100 μm. **C**, Representative images of migration in the HUVECs by wound healing assays (**left**). Scale bars, 100 μm. **Right**, Statistical analysis of reduced area in HUVECs overexpressing KRAS4BG12D (KRAS) and HUVECs overexpressing KRAS4BG12D treated with U0126 (KRAS+U0126) and HUVECs transfected with control adenovirus (CTRL) in wound healing assays. *P* by Mann-Whitney nonparametric test (n=5). The T bars represent SD. **D**, Representative phase-contrast images on beads of HUVECs overexpressing KRAS4B^{G12D} and control in a 3-dimensional fibrin gel angiogenesis assay at days 5, 6, and 7. Scale bar, 100 μm. The number of vascular-like structures (VLSs) around the beads was counted manually, and the lengths of VLSs and area of ECs were quantified. Data (mean±SEM) were obtained from 15 randomly selected beads in each group from 3 individual experiments. *P* by unpaired *t* test α-SMA indicates alpha-smooth muscle actin; CD31, cluster of differentiation 31; CTRL, HUVECs infected with control adenovirus; DAPI, 4',6-diamidino-2-phenylindole; GFP, green fluorescent protein; HUVEC, human umbilical vein endothelial cells; SLUG, SNAI2 snail family transcriptional repressor 2; TAGLN, Transgelin; VE-CAD, vascular endothelial-cadherin; and VWF, von Willebrand factor.

Downloaded from http://ahajournals.org by on November 3, 2021

whether lovastatin reverses EndMT induced by KRAS mutation in ECs, we treated HUVECs overexpressing mutant KRAS with lovastatin and examined EndMT markers by immunofluorescent staining. Induced mesenchymal marker α-SMA was abrogated and the suppressed endothelial marker CD31 was upregulated upon treatment (Figure 7A; Figure XIXA in the Data Supplement). This result was further confirmed by RT-qPCR and Western blot (Figure 7B; Figure XIXB in the Data Supplement). Moreover, we demonstrated that lovastatin reversed the enhanced migration induced by KRAS activation (Figure 7C; Figure XIXC in the Data Supplement). Similarly, we examined whether Lovastatin could reverse EndMT in the *JUP*, *EXPH5*, and *ENG* knockdown HUVECs. As exhibited in Figure 7D, when treated with lovastatin, the mesenchymal markers α-SMA and TAGLN were substantially decreased in all 3 gene knockdown HUVECs, while CD31 was moderately increased in *JUP* and *ENG* knockdown HUVECs (Figure XIXD and XIXE in the Data Supplement). Meanwhile, enhanced migration induced by 3 gene knockdowns was reversed by lovastatin treatment (Figure 7E; Figure XIXC in the Data Supplement). These results collectively demonstrated the role of lovastatin in reversing EndMT induced by either *KRAS* mutations or DNMs in vitro.

Next, we explored whether lovastatin could inhibit EndMT in patient-derived ECs. Isolated bAVM ECs cultured in endothelial medium expressed α-SMA, SLUG (SNAI2, snail family transcriptional repressor 2), and TAGLN. When treated with lovastatin, α-SMA, TAGLN, and SLUG expression was decreased, implying a suppression of EndMT in those cells (Figure 7F; Figure XX in the Data Supplement).

DISCUSSION

Here, we performed DNA sequencing on 219 bAVMs and blood samples of 60 case-unaffected-parental trios. The largest bAVM cohort in the Chinese population enabled the discovery of association between somatic *KRAS* mutation (in 72% cases) and bleeding as the first symptom. The discrepancy in *KRAS* mutation frequency of different studies may be due to different population group, clinical practice, sample status, and the detection techniques.

In addition, we identified 63 DNMs from 60 case-unaffected-parental trios with an average 1.05 (range from 0 to 5) mutations per patient. Previous studies have reported the increase in the number of DNMs with parent's age at conception,[43] but probably due to the limited number of samples, no significant association has been observed in our cohort. Furthermore, no obvious patterns were detected in patients who were carrying over 1 DNM. We note that most of the DNMs are not functional in the disease process. Therefore, only 48 nonsynonymous noncommon DNMs that affect 46 genes were selected for further investigation. We propose that whereas not all variants were disease relevant, some of these mutations would increase the risk or predispose bAVM in individuals. To interrogate the involvement of these genes in bAVM pathogenesis, we pooled these genes together to perform a gene set enrichment type of analysis. We found cell adhesion, cell migration, and cell junction terms enriched in GO analysis, 6 DNM genes significantly enriched in vessel-specific gene expression cluster in tissue-level analysis, and significantly enriched expression of the DNM genes in blood vessel–related cell types through public single-cell database. These imply that a significant number of the DNM genes are potentially associated with bAVM pathogenesis. Based on the variant impact on the protein, we identified crucial DNMs such as *ENG* (a splicing variant), *JUP* (stop codon), and *EXPH5* (recurrence in 2 independent cases with 1 stop codon and 1 missense variant) and showed that alterations in these genes in vitro were associated with EndMT-like change. Moreover, knockdown of *epas1*, 1 of the 6 DNM genes in vessel-specific gene cluster, drived brain vascular malformation and induced cranial hemorrhage in zebrafish. However, more comprehensive in vivo models such as variant heterozygous mouse should be utilized to completely illuminate the effects of the DNMs and corresponding mechanisms in future research.

Patients with DNMs in the prioritized 16 genes were found to be associated with epilepsy as the first symptom. The potential mechanism regarding this observation may need further investigation. However, it is believed that the DNMs occur early in the embryonic development and the cerebrovascular malformations caused by early embryonic development mutations can affect the blood supply to the cortex chronically leading to cortical dysgenesis, which often results in epilepsy.[44] Moreover, patient A095 had 2 in phase DNMs in the *DLGAP3* gene, where substitution at 2 adjacent nucleotides occurred resulting in the change of 2 amino acids (Figure XXI in the Data Supplement). Previous study has generated *SAPAP3(DLGAP3)*-mutant mice that showed deficiency in corticostriatal synapses and led to obsessive compulsive disorder–like behaviors.[45] Further follow-up will be needed to study the effects of these 2 variants.

We observed EndMT in simplex bAVM and propose that the identified DNMs and somatic *KRAS* mutations may convergently provoke EndMT, but additional studies would be needed to understand potential cross talk between these alterations. EndMT is a collective course in which gradations (ie, partial versus more complete EndMT, reversible, transient) and extent of reduced endothelial markers versus increased mesenchymal markers should be considered.[46] Different patterns of EndMT were reported in various physiological and pathological processes.[20,39] In bAVMs, by utilizing single-cell analysis, we found 3 subgroups of ECs, and each group expressed different pattern of mesenchymal markers, indicating a complicated EndMT in bAVM endothelium. Further investigation would be needed to decipher the heterogeneity in vivo. Interestingly, we found *KRAS*-mutant bAVMs were prone to rupture. We speculated this correlation could be explained by the severe EndMT induced by the *KRAS* mutation. It is also in consistency with our previous finding that a more prominent EndMT was correlated with microhemorrhage of bAVMs.[47]

Downloaded from http://ahajournals.org by on November 3, 2021

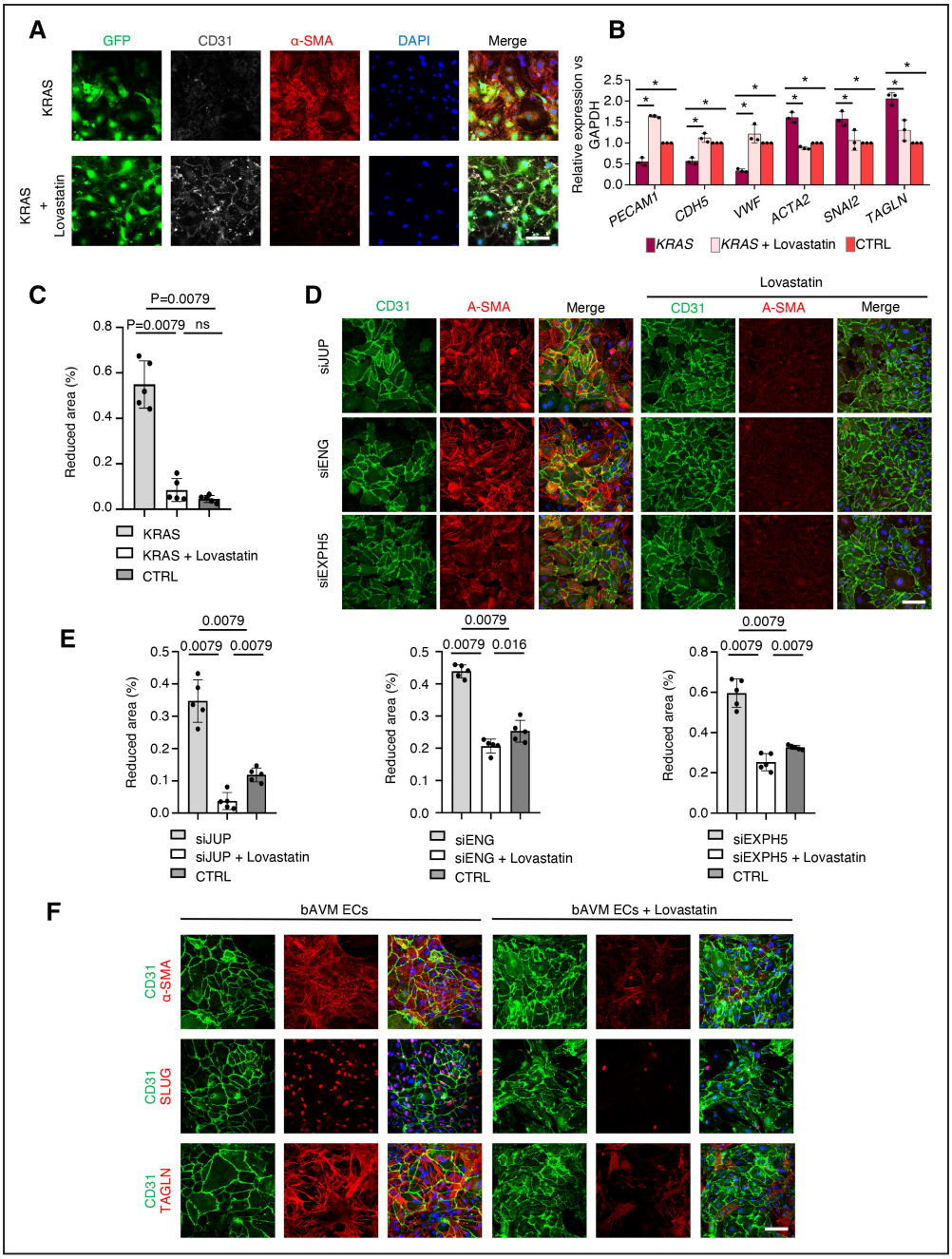


Figure 7. In vitro and ex vivo studies demonstrated repurposing lovastatin that targets endothelial-to-mesenchymal transition as a potential treatment of brain arteriovenous malformations (bAVMs).

A, Immunofluorescence staining of CD31 and α-SMA in human umbilical vein endothelial cells (HUVECs) overexpressing KRAS4B^{G12D} and HUVECs overexpressing KRAS4B^{G12D} treated with lovastatin. Scale bar, 100 μm. **B**, Expression of endothelial and mesenchymal markers in HUVECs overexpressing KRAS4B^{G12D}, HUVECs overexpressing KRAS4B^{G12D} treated with lovastatin, and control as shown by real-time PCR (n=3). The P values of * mark are the following: KRAS vs CTRL (PECAM1: P=0.0013; CDH5: P=6.8×10^{-4}; VWF: P=9.6×10^{-6}; ACTA2: P=0.0011; SNAI2: P=0.0050; TAGLN: P=2.3×10^{-4}); KRAS vs Kras+lovastatin (PECAM1: P=4.9×10^{-5}; CDH5: P=0.0018; VWF: P=0.0023; ACTA2: P=6.2×10^{-4}; SNAI2: P=0.040; TAGLN: P=0.011). Analyzed by unpaired *t* test. The T bars represent SD. **C**, Statistical analysis of reduced area in HUVECs overexpressing KRAS4B^{G12D} (KRAS) and HUVECs overexpressing KRAS4B^{G12D} treated with lovastatin (KRAS+lovastatin) and HUVECs transfected with control adenovirus (CTRL) in wound healing assays. The T bars represent SD. *P* by Mann-Whitney nonparametric test (n=5). **D**, Expression of endothelial marker CD31 and mesenchymal marker α-SMA in HUVECs with *JUP*, *ENG*, and *EXPH5* knockdown and with lovastatin treatment by immunofluorescence staining. Scale bar, 100 μm. **E**, Statistical analysis of reduced area in HUVECs with *JUP*, *ENG*, and *EXPH5* knockdown (siJUP/ENG/EXHP5), knockdown HUVECs treated with lovastatin (siJUP/ENG/EXHP5+lovastatin), and HUVECs transfected with control siRNA (CTRL) in wound healing assays. The T bars represent SD. *P* by Mann-Whitney nonparametric test (n=5). **F**, Representative immunofluorescence staining images of primary endothelial cells (ECs) derived from bAVM. The overexpressed mesenchymal markers (α-SMA, SLUG, and TAGLN) are observed in these cells. Lovastatin treatment inhibits the expression of these mesenchymal markers. Green, CD31; red, mesenchymal markers; blue, DAPI. Scale bar, 100 μm. CTRL in **A**, **B** and **C** indicate HUVECs infected with control adenovirus. CTRL in **D** and **E** indicate HUVECs transfected with control siRNA. α-SMA indicates alpha-smooth muscle actin; CD31, cluster of differentiation 31; DAPI, 4',6-diamidino-2-phenylindole; GFP, green fluorescent protein; HUVEC, human umbilical vein endothelial cells; SLUG, SNAI2 snail family transcriptional repressor 2; TAGLN, Transgelin; and VWF, von Willebrand factor.

Downloaded from http://ahajournals.org by on November 3, 2021

Since EndMT is ubiquitously observed in bAVMs with heterogeneous genetic background, we argue that the EndMT, rather than the KRAS or ERK pathways, is playing the most crucial role in the development of bAVMs, and future studies could concentrate on targeting EndMT but not limited to KRAS or ERK pathways to R&D bAVM novel therapeutic drugs. The 3-hydroxy-3-methylglutaryl coenzyme A reductase inhibitors (statins) have widely been in clinical use for the reduction of total cholesterol and LDL-C (low-density lipoprotein cholesterol) levels and have been shown to be safe.[48] Here, we presented the efficacy of lovastatin in reversing EndMT using in vitro and ex vivo experiments, providing new preclinical evidence for future clinical trials that might benefit numerous patients. Regarding the mechanism, it has previously been revealed that TGF-β signaling and oxidative stress are able to promote the EndMT process and lovastatin could significantly suppress TGF-β signaling and oxidative stress.[37,42] Subsequent in vitro study found that lovastatin could suppress high glucose–induced EndMT in glomerular ECs through downregulating TGF-β1 expression and Smad2/3 phosphorylation.[42] In addition, lovastatin could reduce malondialdehyde and superoxide dismutase decreasing oxidative stress in the kidney of diabetic mouse.[42] Therefore, we suspect that lovastatin may alleviate EndMT in ECs through the inhibition of TGF-β signaling. However, further experimental studies will be needed to consolidate the molecular mechanisms before clinical applications.

ARTICLE INFORMATION

Received February 2, 2021; revision received September 3, 2021; accepted September 16, 2021.

Affiliations

Neurosurgery, Beijing Tiantan Hospital (H.L., R.H., W.F., Y.J., Jiancong Weng, Z.Y., Jie Wang, H.X., S.W., J.Z., Y.C.) and Beijing Neurosurgical Institute (Y.C.), Capital Medical University, China. China National Clinical Research Center for Neurological Diseases, Beijing, China (H.L., R.H., W.F., Y.J., Jiancong Weng, Z.Y., Jie Wang, H.X., S.W., J.Z., Y.C.). Division of Life Science, State Key Laboratory of Molecular Neuroscience (Y.N., Q.Z., D.S., Z.W., Jiguang Wang) and Chemical and Biological Engineering (B.J., Y.Y., Jiguang Wang), the Hong Kong University of Science and Technology (B.J.,Y.Y.), Clear Water Bay, Kowloon, Hong Kong SAR, China. Greater Bay Biomedical Innocenter, Shenzhen Bay Laboratory, Shenzhen, China (Z.W.). Hong Kong Center for Neurodegenerative Diseases, Hong Kong Science Park, Hong Kong SAR, China (Jiguang Wang). Beijing Advanced Innovation Center for Genomics, Biomedical Pioneering Innovation Center, Peking-Tsinghua Center for Life Sciences (L.D.) and School of Life Sciences (L.D.), Peking University, Beijing, China. School of Life Sciences, Tsinghua-Peking Center for Life Sciences, Tsinghua University, Beijing, China (J.L.).

Sources of Funding

This article is funded by the project "Genomics Platform Construction for Chinese Major Brain Disease-AVM" (No. PXM2019_026280_000002-AVM), Beijing Advanced Innovation Center for Big Data-based Precision Medicine (PXM2020_014226_000066), NSFC Excellent Young Scientists Fund (No. 31922088), Hong Kong RGC Fund (C6002-17GF), Hong Kong Epigenomics Project (LKCCFL18SC01-E), and the Hong Kong ITC Fund (ITCPD/17-9). This research made use of the computing resources of the X-GPU cluster supported by the Hong Kong Research Grant Council Collaborative Research Fund (C6021-19EF). Our research also received funding from Beijing Advanced Innovation Center for Big Data-based Precision Medicine (PXM2020_014226_000066) and Hong Kong Epigenomics Project (LKCCFL18SC01-E).

Disclosures

None.

Supplemental Materials

Expanded Methods
Data Supplement Figures I–XXI
Data Supplement Tables I–VIII
References [49–59]

REFERENCES

1. Darsaut TE, Guzman R, Marcellus ML, Edwards MS, Tian L, Do HM, Chang SD, Levy RP, Adler JR, Marks MP, et al. Management of pediatric intracranial arteriovenous malformations: experience with multimodality therapy. *Neurosurgery*. 2011;69:540–556; discussion 556. doi: 10.1227/NEU.0b013e3182181c00
2. Nikolaev SI, Vetiska S, Bonilla X, Boudreau E, Jauhiainen S, Rezai Jahromi B, Khyzha N, DiStefano PV, Suutarinen S, Kiehl TR, et al. Somatic activating KRAS mutations in arteriovenous malformations of the brain. *N Engl J Med*. 2018;378:250–261. doi: 10.1056/NEJMoa1709449
3. Al-Olabi L, Polubothu S, Dowsett K, Andrews KA, Stadnik P, Joseph AP, Knox R, Pittman A, Clark G, Baird W, et al. Mosaic RAS/MAPK variants cause sporadic vascular malformations which respond to targeted therapy. *J Clin Invest*. 2018;128:1496–1508. doi: 10.1172/JCI98589
4. Hong T, Yan Y, Li J, Radovanovic I, Ma X, Shao YW, Yu J, Ma Y, Zhang P, Ling F, et al. High prevalence of KRAS/BRAF somatic mutations in brain and spinal cord arteriovenous malformations. *Brain*. 2019;142:23–34. doi: 10.1093/brain/awy307
5. Priemer DS, Vortmeyer AO, Zhang S, Chang HY, Curless KL, Cheng L. Activating KRAS mutations in arteriovenous malformations of the brain: frequency and clinicopathologic correlation. *Hum Pathol*. 2019;89:33–39. doi: 10.1016/j.humpath.2019.04.004
6. Oka M, Kushamae M, Aoki T, Yamaguchi T, Kitazato K, Abekura Y, Kawamata T, Mizutani T, Miyamoto S, Takagi Y. KRAS G12D or G12V mutation in human brain arteriovenous malformations. *World Neurosurg*. 2019;126:e1365–e1373. doi: 10.1016/j.wneu.2019.03.105
7. Goss JA, Huang AY, Smith E, Konczyk DJ, Smits PJ, Sudduth CL, Stapleton C, Patel A, Alexandrescu S, Warman ML, et al. Somatic mutations in intracranial arteriovenous malformations. *PLoS 1*. 2019;14:e0226852. doi: 10.1371/journal.pone.0226852
8. Fish JE, Flores Suarez CP, Boudreau E, Herman AM, Gutierrez MC, Gustafson D, DiStefano PV, Cui M, Chen Z, De Ruiz KB, et al. Somatic Gain of KRAS function in the endothelium is sufficient to cause vascular malformations that require MEK but Not PI3K signaling. *Circ Res*. 2020;127:727–743. doi: 10.1161/CIRCRESAHA.119.316500
9. Yao J, Wu X, Zhang D, Wang L, Zhang L, Reynolds EX, Hernandez C, Boström KI, Yao Y. Elevated endothelial Sox2 causes lumen disruption and cerebral arteriovenous malformations. *J Clin Invest*. 2019;129:3121–3133. doi: 10.1172/JCI125965
10. Chen W, Sun Z, Han Z, Jun K, Camus M, Wankhede M, Mao L, Arnold T, Young WL, Su H. De novo cerebrovascular malformation in the adult mouse after endothelial Alk1 deletion and angiogenic stimulation. *Stroke*. 2014;45:900–902. doi: 10.1161/STROKEAHA.113.003655
11. Ethan W, David M, Zhengda S, Daniel C. Abstract 128: RNA-seq based non-invasive endovascular biopsy of brain arteriovenous malformations. *Stroke*. 2020;51:A128–A128. doi: 10.1161/str.51.suppl_1.128
12. Hauer AJ, Kleinloog R, Giuliani F, Rinkel GJE, de Kort GA, Berkelbach van der Sprenkel JW, van der Zwan A, Gosselaar PH, van Rijen PC, de Boer-Bergsma JJ, et al. RNA-sequencing highlights inflammation and impaired integrity of the vascular wall in brain arteriovenous malformations. *Stroke*. 2020;51:268–274. doi: 10.1161/STROKEAHA.119.025657
13. Mu Q, Chen Y, Wang J. Deciphering brain complexity using single-cell sequencing. *Genomics Proteomics Bioinformatics*. 2019;17:344–366. doi: 10.1016/j.gpb.2018.07.007
14. Orsenigo F, Conze LL, Jauhiainen S, Corada M, Lazzaroni F, Malinverno M, Sundell V, Cunha SI, Brännström J, Globisch MA, et al. Mapping endothelial-cell diversity in cerebral cavernous malformations at single-cell resolution. *Elife*. 2020;9:e61413. doi: 10.7554/eLife.61413
15. Rivière JB, Mirzaa GM, O'Roak BJ, Beddaoui M, Alcantara D, Conway RL, St-Onge J, Schwartzentruber JA, Gripp KW, Nikkel SM, et al; Finding of Rare Disease Genes (FORGE) Canada Consortium. De novo germline and postzygotic mutations in AKT3, PIK3R2 and PIK3CA cause a spectrum of related megalencephaly syndromes. *Nat Genet*. 2012;44:934–940. doi: 10.1038/ng.2331
16. Jin ZB, Li Z, Liu Z, Jiang Y, Cai XB, Wu J. Identification of de novo germline mutations and causal genes for sporadic diseases using trio-based whole-exome/genome sequencing. *Biol Rev Camb Philos Soc*. 2018;93:1014–1031. doi: 10.1111/brv.12383

Downloaded from http://ahajournals.org by on November 3, 2021

17. Vanlandewijck M, He L, Mäe MA, Andrae J, Ando K, Del Gaudio F, Nahar K, Lebouvier T, Laviña B, Gouveia L, et al. A molecular atlas of cell types and zonation in the brain vasculature. *Nature*. 2018;554:475–480. doi: 10.1038/nature25739
18. Hawrylycz MJ, Lein ES, Guillozet-Bongaarts AL, Shen EH, Ng L, Miller JA, van de Lagemaat LN, Smith KA, Ebbert A, Riley ZL, et al. An anatomically comprehensive atlas of the adult human brain transcriptome. *Nature*. 2012;489:391–399. doi: 10.1038/nature11405
19. Piera-Velazquez S, Jimenez SA. Endothelial to mesenchymal transition: role in physiology and in the pathogenesis of human diseases. *Physiol Rev*. 2019;99:1281–1324. doi: 10.1152/physrev.00021.2018
20. Maddaluno L, Rudini N, Cuttano R, Bravi L, Giampietro C, Corada M, Ferrarini L, Orsenigo F, Papa E, Boulday G, et al. EndMT contributes to the onset and progression of cerebral cavernous malformations. *Nature*. 2013;498:492–496. doi: 10.1038/nature12207
21. McAllister KA, Grogg KM, Johnson DW, Gallione CJ, Baldwin MA, Jackson CE, Helmbold EA, Markel DS, McKinnon WC, Murrell J. Endoglin, a TGF-beta binding protein of endothelial cells, is the gene for hereditary haemorrhagic telangiectasia type 1. *Nat Genet*. 1994;8:345–351. doi: 10.1038/ng1294-345
22. Johnson DW, Berg JN, Baldwin MA, Gallione CJ, Marondel I, Yoon SJ, Stenzel TT, Speer M, Pericak-Vance MA, Diamond A, et al. Mutations in the activin receptor-like kinase 1 gene in hereditary haemorrhagic telangiectasia type 2. *Nat Genet*. 1996;13:189–195. doi: 10.1038/ng0696-189
23. Roach JC, Glusman G, Smit AF, Huff CD, Hubley R, Shannon PT, Rowen L, Pant KP, Goodman N, Bamshad M, et al. Analysis of genetic inheritance in a family quartet by whole-genome sequencing. *Science*. 2010;328:636–639. doi: 10.1126/science.1186802
24. Nachman MW, Crowell SL. Estimate of the mutation rate per nucleotide in humans. *Genetics*. 2000;156:297–304. doi: 10.1093/genetics/156.1.297
25. Jónsson H, Sulem P, Kehr B, Kristmundsdottir S, Zink F, Hjartarson E, Hardarson MT, Hjorleifsson KE, Eggertsson HP, Gudjonsson SA, et al. Parental influence on human germline de novo mutations in 1,548 trios from Iceland. *Nature*. 2017;549:519–522. doi: 10.1038/nature24018
26. Kryukov GV, Pennacchio LA, Sunyaev SR. Most rare missense alleles are deleterious in humans: implications for complex disease and association studies. *Am J Hum Genet*. 2007;80:727–739. doi: 10.1086/513473
27. Parker HR, Li Z, Sheinin H, Lauzon G, Pasdar M. Plakoglobin induces desmosome formation and epidermoid phenotype in N-cadherin-expressing squamous carcinoma cells deficient in plakoglobin and E-cadherin. *Cell Motil Cytoskeleton*. 1998;40:87–100. doi: 10.1002/(SICI)1097-0169(1998)40:1<87::AID-CM8>3.0.CO;2-C
28. Bayrak-Toydemir P, Mao R, Lewin S, McDonald J. Hereditary hemorrhagic telangiectasia: an overview of diagnosis and management in the molecular era for clinicians. *Genet Med*. 2004;6:175–191. doi: 10.1097/01.gim.0000132689.25644.7c
29. Pece N, Vera S, Cymerman U, White RI Jr, Wrana JL, Letarte M. Mutant endoglin in hereditary hemorrhagic telangiectasia type 1 is transiently expressed intracellularly and is not a dominant negative. *J Clin Invest*. 1997;100:2568–2579. doi: 10.1172/JCI119800
30. McGrath JA, Stone KL, Begum R, Simpson MA, Dopping-Hepenstal PJ, Liu L, McMillan JR, South AP, Pourreyron C, McLean WH, et al. Germline Mutation in EXPH5 implicates the Rab27B effector protein Slac2-b in inherited skin fragility. *Am J Hum Genet*. 2012;91:1115–1121. doi: 10.1016/j.ajhg.2012.10.012
31. Sherry ST, Ward M, Sirotkin K. dbSNP-database for single nucleotide polymorphisms and other classes of minor genetic variation. *Genome Res*. 1999;9:677–679.
32. Cao Y, Li L, Xu M, et al. The ChinaMAP analytics of deep whole genome sequences in 10,588 individuals. *Cell Research*. 2020;30:717–731. doi: 10.1038/s41422-020-0322-9
33. Peng J, Zhang L, Drysdale L, Fong G-H. The transcription factor EPAS-1/hypoxia-inducible factor 2α plays an important role in vascular remodeling. *Proceedings of the National Academy of Sciences*. 2000;97:8386 LP–8391. doi: 10.1073/pnas.140087397
34. Zanetti M, Braghetta P, Sabatelli P, Mura I, Doliana R, Colombatti A, Volpin D, Bonaldo P, Bressan GM. EMILIN-1 deficiency induces elastogenesis and vascular cell defects. *Mol Cell Biol*. 2004;24:638–650. doi: 10.1128/MCB.24.2.638-650.2004
35. Zacchigna L, Vecchione C, Notte A, Cordenonsi M, Dupont S, Maretto S, Cifelli G, Ferrari A, Maffei A, Fabbro C, et al. Emilin1 links TGF-beta maturation to blood pressure homeostasis. *Cell*. 2006;124:929–942. doi: 10.1016/j.cell.2005.12.035
36. Franzén O, Gan LM, Björkegren JLM. PanglaoDB: a web server for exploration of mouse and human single-cell RNA sequencing data. *Database (Oxford)*. 2019;2019:baz046. doi: 10.1093/database/baz046
37. Evrard SM, Lecce L, Michelis KC, Nomura-Kitabayashi A, Pandey G, Purushothaman KR, d'Escamard V, Li JR, Hadri L, Fujitani K, et al. Endothelial to mesenchymal transition is common in atherosclerotic lesions and is associated with plaque instability. *Nat Commun*. 2016;7:11853. doi: 10.1038/ncomms11853
38. Gerri C, Marass M, Rossi A, Stainier DYR. Hif-1α and Hif-2α regulate hemogenic endothelium and hematopoietic stem cell formation in zebrafish. *Blood*. 2018;131:963–973. doi: 10.1182/blood-2017-07-797795
39. Welch-Reardon KM, Wu N, Hughes CC. A role for partial endothelial-mesenchymal transitions in angiogenesis? *Arterioscler Thromb Vasc Biol*. 2015;35:303–308. doi: 10.1161/ATVBAHA.114.303220
40. Xiao L, Dudley AC. Fine-tuning vascular fate during endothelial-mesenchymal transition. *J Pathol*. 2017;241:25–35. doi: 10.1002/path.4814
41. Potenta S, Zeisberg E, Kalluri R. The role of endothelial-to-mesenchymal transition in cancer progression. *Br J Cancer*. 2008;99:1375–1379. doi: 10.1038/sj.bjc.6604662
42. Ma Z, Zhu L, Liu Y, Wang Z, Yang Y, Chen L, Lu Q. Lovastatin alleviates endothelial-to-mesenchymal transition in glomeruli via suppression of oxidative stress and TGF-β1 signaling. *Front Pharmacol*. 2017;8:473. doi: 10.3389/fphar.2017.00473
43. Goldmann JM, Veltman JA, Gilissen C. De Novo mutations reflect development and aging of the human germline. *Trends Genet*. 2019;35:828–839. doi: 10.1016/j.tig.2019.08.005
44. Comi AM. Pathophysiology of sturge-weber syndrome. *J Child Neurol*. 2003;18:509–516. doi: 10.1177/08830738030180080701
45. Welch JM, Lu J, Rodriguiz RM, Trotta NC, Peca J, Ding JD, Feliciano C, Chen M, Adams JP, Luo J, et al. Cortico-striatal synaptic defects and OCD-like behaviours in Sapap3-mutant mice. *Nature*. 2007;448:894–900. doi: 10.1038/nature06104
46. Kovacic JC, Dimmeler S, Harvey RP, Finkel T, Aikawa E, Krenning G, Baker AH. Endothelial to mesenchymal transition in cardiovascular disease: JACC State-of-the-Art Review. *J Am Coll Cardiol*. 2019;73:190–209. doi: 10.1016/j.jacc.2018.09.089
47. Weilun F, Ran H, Zihan Y, et al. Mesenchymal behavior of the endothelium promoted by SMAD6 downregulation is associated with brain arteriovenous malformation microhemorrhage. *Stroke*. 2020;51:2197–2207.
48. Stein EA, Illingworth DR, Kwiterovich PO, et al. Efficacy and safety of lovastatin in adolescent males with heterozygous familial hypercholesterolemia. A randomized controlled trial. *Journal of the American Medical Association*. 1999.
49. Shovlin CL, Guttmacher AE, Buscarini E, Faughnan ME, Hyland RH, Westermann CJ, Kjeldsen AD, Plauchu H. Diagnostic criteria for hereditary hemorrhagic telangiectasia (Rendu-Osler-Weber syndrome). *Am J Med Genet*. 2000;91:66–67. doi: 10.1002/(sici)1096-8628(20000306)91:1<66::aid-ajmg12>3.0.co;2-p
50. Korsunsky I, Millard N, Fan J, Slowikowski K, Zhang F, Wei K, Baglaenko Y, Brenner M, Loh PR, Raychaudhuri S. Fast, sensitive and accurate integration of single-cell data with harmony. *Nat Methods*. 2019;16:1289–1296. doi: 10.1038/s41592-019-0619-0
51. Westerfield M. A guide for the laboratory use of zebrafish (Danio rerio). *The Zebrafish Book*. 2000;4.
52. Jin SW, Beis D, Mitchell T, Chen JN, Stainier DY. Cellular and molecular analyses of vascular tube and lumen formation in zebrafish. *Development*. 2005;132:5199–5209. doi: 10.1242/dev.02087
53. Tian Y, Xu J, Feng S, et al. The first wave of T lymphopoiesis in zebrafish arises from aorta endothelium independent of hematopoietic stem cells. *J Exp Med*. 2017.
54. Metelo AM, Noonan HR, Li X, Jin Y, Baker R, Kamentsky L, Zhang Y, van Rooijen E, Shin J, Carpenter AE, et al. Pharmacological HIF2α inhibition improves VHL disease-associated phenotypes in zebrafish model. *J Clin Invest*. 2015;125:1987–1997. doi: 10.1172/JCI73665
55. Wang J, Cazzato E, Ladewig E, Frattini V, Rosenbloom DI, Zairis S, Abate F, Liu Z, Elliott O, Shin YJ, et al. Clonal evolution of glioblastoma under therapy. *Nat Genet*. 2016;48:768–776. doi: 10.1038/ng.3590
56. Waterhouse A, Bertoni M, Bienert S, Studer G, Tauriello G, Gumienny R, Heer FT, de Beer TAP, Rempfer C, Bordoli L, et al. SWISS-MODEL: homology modelling of protein structures and complexes. *Nucleic Acids Res*. 2018;46:W296–W303. doi: 10.1093/nar/gky427
57. Case DA, Babin V, Berryman JT, et al. AMBER14. *AMBER 14*. 2014.
58. Wolf FA, Angerer P, Theis FJ. SCANPY: large-scale single-cell gene expression data analysis. *Genome Biol*. 2018;19:15. doi: 10.1186/s13059-017-1382-0
59. Gerstung M, Beisel C, Rechsteiner M, Wild P, Schraml P, Moch H, Beerenwinkel N. Reliable detection of subclonal single-nucleotide variants in tumour cell populations. *Nat Commun*. 2012;3:811. doi: 10.1038/ncomms1814

Downloaded from http://ahajournals.org by on November 3, 2021